Two-Photon Driven Kerr Resonator for Quantum Annealing with Three-Dimensional Circuit QED

Peng Zhao,[1] Zhenchuan Jin,[1] Peng Xu,[1] Xinsheng Tan,[1] Haifeng Yu,[1,2,*] and Yang Yu[1,2]

[1]*National Laboratory of Solid State Microstructures, School of Physics, Nanjing University, Nanjing 210093, China*

[2]*Synergetic Innovation Center of Quantum Information & Quantum Physics, University of Science and Technology of China, Hefei, Anhui 230026, China*

We propose a realizable circuit QED architecture for engineering states of a superconducting resonator off-resonantly coupled to an ancillary superconducting qubit. The qubit-resonator dispersive interaction together with a microwave drive applied to the qubit gives rise to a Kerr resonator with two-photon driving that enables us to efficiently engineer the quantum state of the resonator, such as generation of the Schrödinger cat states for resonator-based universal quantum computation. Moreover, the presented architecture is easily scalable for solving an optimization problem mapped into the Ising spin-glass model and thus serves as a platform for quantum annealing. Although various scalable architectures with superconducting qubits have been proposed for realizing a quantum annealer, the existing annealers are currently limited to the coherent time of the qubits. Here, based on the protocol for realizing a two-photon driven Kerr resonator in three-dimensional circuit QED (3D cQED), we propose a flexible and scalable hardware for implementing a quantum annealer that combines the advantage of the long coherence times attainable in 3D cQED and the recently proposed resonator-based Lechner-Hauke-Zoller (LHZ) scheme. In the proposed resonator-based LHZ annealer, each spin is encoded in the subspace formed by two coherent states of the 3D microwave superconducting resonator with opposite phase and thus the fully connected Ising model is mapped onto the network of the resonator with local tunable three-resonator interaction. This hardware architecture provides a promising physical platform for realizing a quantum annealer with improved coherence.

I. INTRODUCTION

The parametrically driven anharmonic oscillator, which is usually modeled by a Kerr resonator with two-photon driving [1,2], has been shown to display rich physics and thus has been studied extensively [3–12]. In a system consisting of a Kerr resonator with two-photon driving operating in the quantum regime, where the Kerr nonlinearity is stronger than the photon decay rate, various schemes have been proposed for engineering the quantum state of the resonator [3,5,7,13–15]. Among these efforts, preparing the Schrödinger cat state, i.e., superpositions of two large coherent states with opposite phases, has been extensively investigated for the development of quantum metrology [16] and quantum information processing [16,17]. Moreover, driven by the pursuit towards practical quantum information processing, quantum annealing [18] was proposed as a quantum-enhanced optimizer that aims to efficiently solve Ising problems [19,20]; this resonator system

has attracted increasing attention owing to its coupled network, which offers a new paradigm for the quantum annealer [13,21–23]. In this paradigm, the quantum information is encoded and protected in the continuous variable system, i.e., resonator, and a series of theoretical studies have shown the robustness of this paradigm with respect to dissipation and noise [22,23].

Typically, the Kerr nonlinearity can be induced by inserting a nonlinear medium (the Kerr medium) into a resonator. For example, in the optical (nanomechanical) resonator system, the Kerr nonlinearity can be produced by the atom-photon (atom/photon-phonon) interaction in a resonator [24–26]. In the quantum regime, the Kerr nonlinear resonator has generally been considered to be treated as nonlinear quantum scissors (NQS) [27] for exploring quantum effects, such as a photon blockade, in these systems. Moreover, by combining this NQS system with a multi-photon process [5,27] or multi-photon dissipating process [28,29], one can control the quantum state of the resonator [5,30]. However, the induced Kerr nonlinearity is usually smaller than the dissipation rate in optical

---
*hfyu@nju.edu.cn

and nanomechanical systems, hindering further study of the quantum regime of this system. Recent advances in artificial solid-state systems, especially in the circuit QED (cQED) system, provide an alternative approach to easily gain access to this fascinating quantum regime at a single-photon level [31].

In the context of cQED, the Kerr resonator is realized by using a superconducting resonator with an embedded Josephson junction [32,33], which is almost an ideal nondissipative nonlinear element [34]. Therefore, this gives rise to two main approaches to realize the two-photon driven Kerr resonator in the cQED architecture. One approach to realizing the system is to use a superconducting coplanar resonator terminated by a flux-pumped superconducting quantum interference device (SQUID) [35–37]. Alternatively, a recent experimental work has shown a nonlinear driven-dissipation approach by using a 3D microwave resonator coupled to a fixed-frequency transmon qubit and by an external microwave drive applied to the qubit at the resonator frequency [30]. For the latter approach, remarkably, a 3D microwave resonator with high quality factors has been experimentally demonstrated [38], enabling storage times approaching seconds [39] and thus favoring the quantum information processing based on the 3D microwave superconducting resonator [17,40]. However, it is noted that this approach is implemented by using a two-photon driven-dissipation process where the engineered nonlinear (two-photon) decay rate should be significantly larger than the single-photon decay rate of the cavity, which still remains an important challenge to be overcome [30]. This current limitation suggests investigating another relatively easily realizable approach that also exploits the large coherence times of the 3D microwave superconducting resonator.

In this work we propose an experimentally feasible protocol for realizing a two-photon driven Kerr resonator in a cQED architecture, which, in principle, is compatible with the 3D cQED architecture with high coherence. The Kerr resonator with two-photon driving, which lie at its heart, is realized via off-resonantly coupling a resonator to an ancillary microwave-driven superconducting qubit. In our setting, the superconducting qubit is treated as a quantum three-level system that is initially in its ground state, which remains unexcited in the whole process, minimizing the effect of the qubit decoherence. Moreover, based on our protocol for realizing a two-photon driven Kerr resonator, we apply a combination of the recently proposed resonator-based Lechner-Hauke-Zoller (LHZ) annealer [22] and the 3D cQED architecture that allows a flexible and scalable hardware architecture with long coherence times for the LHZ annealer. In our setting, each spin in the LHZ-represented Ising problem is encoded in the degenerate ground subspace of the two-photon driven Kerr resonator formed by two coherent states of opposite phases, and the four-body constraints, which are decomposed into two three-body constraints, are physical implemented with the use of transmon-qubit-mediated tunable three-resonator interactions.

II. THE SYSTEM AND HAMILTONIAN

In order to construct a cQED platform for engineering the quantum state of the resonator, and further implementing quantum annealing, here we introduce two major ingredients, a two-photon driven Kerr resonator, which allows us to create a nonclassical state of the resonator, such as Schrödinger cat states, and the tunable resonance three-resonator interaction. Meanwhile, we also aim to exploit the long coherence of the 3D superconducting resonator, so the presented platform should be compatible with the 3D architecture. With these aims in mind, in the following discussion: (i) We propose a scheme to realize the two-photon driven Kerr resonator in a qubit-resonator system, where the resonator is coupled to a superconducting qubit and the qubit is driven by a coherent microwave drive applied at a well-chosen frequency, as shown in Fig. 1. (ii) We show that a tunable resonance three-resonator interaction can be induced by coupling resonators to a transmon qubit, where the qubit mode decouples from these resonator modes and mediates the three-resonator interaction by applying a suitable pump mode on it, as shown in Fig. 3. In doing so, we present a thorough description of the two ingredients for the coupled network of two-photon driven Kerr resonators. We now turn to the presentation of the quantitative derivation.

A. Kerr nonlinear resonator with two-photon driving

As shown in Fig. 1(a), we consider a system consisting of a resonator coupled to a quantum three-level system (qutrit), for which the transitions $|g\rangle \leftrightarrow |e\rangle$ and $|e\rangle \leftrightarrow |f\rangle$ of the qutrit are off-resonantly coupled with the resonator, while the $|g\rangle \leftrightarrow |f\rangle$ transition is coupled to a coherent microwave drive with a frequency of nearly twice the resonator frequency. The proposed scheme can be physically realized in a cQED architecture consisting of a superconducting resonator capacitively coupled to a superconducting qubit, which can be achieved by using a flux qubit [41,42] or a fluxoninum qubit [43], as depicted in Fig. 1(b). Here, we focus on the lowest three energy levels of the superconducting qubit and thus we treat the qubit as a three-level system (qutrit) (see Appendix A for details of the cQED system). After applying the rotating-wave approximation (RWA), the full system can be described by the Hamiltonian ($\hbar = 1$, throughout the paper)

$$H = H_0 + H_I + H_d, \tag{1}$$

where

$$H_0 = \omega_c a^\dagger a + \sum_{j=g,e,f} \epsilon_j |j\rangle\langle j| \tag{2}$$
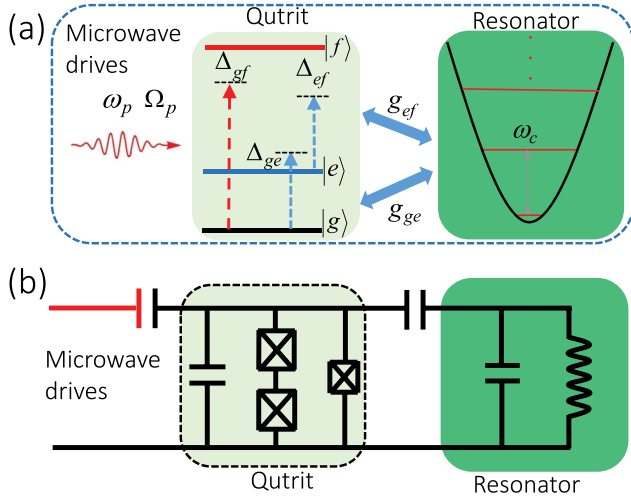
FIG. 1. (a) General proposal for realizing the two-photon driven Kerr resonator, where the transitions $|g\rangle \leftrightarrow |e\rangle$ and $|e\rangle \leftrightarrow |f\rangle$ of the quantum three-level system (qutrit) are dispersively coupled with the resonator, while the $|g\rangle \leftrightarrow |f\rangle$ transition is driven off-resonantly by a coherent microwave drive of frequency at nearly twice the resonator frequency. (b) Circuit diagram of the proposed cQED system for realizing the proposal, where the superconducting resonator is capacitively coupled to a capacitively shunted superconducting flux qubit that is driven by a coherent microwave drive.

describes the free Hamiltonian of the resonator, the qutrit,

$$H_I = g_{ge}(|g\rangle\langle e|a^\dagger + |e\rangle\langle g|a) + g_{ef}(|e\rangle\langle f|a^\dagger + |f\rangle\langle e|a),$$ (3)

describes the qutrit-resonator interaction, and

$$H_d = \Omega_p(e^{i\omega_p t}|g\rangle\langle f| + e^{-i\omega_p t}|f\rangle\langle g|)$$ (4)

describes the time-dependent drive of the qutrit. Above, $a^\dagger$ and a are the creation and annihilation operators, respectively, for the resonator of frequency ω_c. ϵ_j ($j = g, e, f$) is the transition frequency of the qutrit from the ground to the excited state $|j\rangle$. g_{ge} and g_{ef} denote the qutrit-resonator coupling strengths and Ω_p is the real amplitude of the microwave drives at frequency $\omega_p \approx 2\omega_c$. For simplicity, we define $\epsilon_g = 0$ in the following discussion.

We consider that our system operates in the dispersive regime, where the qutrit is far detuned from the resonator $|\Delta_{jk}| = |(|\epsilon_j - \epsilon_k|) - \omega_c| \gg g_{jk}$ and also the microwave drive $|\Delta'_d| = |\epsilon_f - \omega_p| \gg \Omega_p$. In this situation, the systemic Hamiltonian H can be well approximated by the effective Hamiltonian [44–46]

$$H_{\mathrm{eff}} = \tilde{\omega}_c a^\dagger a + K a^{\dagger 2} a^2 - P(a^{\dagger 2} e^{-i\omega_p t} + a^2 e^{i\omega_p t}),$$ (5)

where $\tilde{\omega}_c = \omega_c + S$ is the renormalized resonator frequency

$$S = -\frac{g_{ge}^2}{\Delta_{ge}} + \frac{g_{ge}^4}{\Delta_{ge}^3}.$$ (6)

The second term denotes the qutrit-induced self-Kerr nonlinearity of the resonator with

$$K = -\frac{g_{ge}^2 g_{ef}^2}{\Delta_{ge}^2(\Delta_{ge} + \Delta_{ef})} + \frac{g_{ge}^4}{\Delta_{ge}^3}.$$ (7)

The last term represents a two-photon drive of amplitude

$$P = -\frac{g_{ge} g_{ef} \Omega_p}{\Delta_{ge}(\epsilon_f - \omega_p)}$$ (8)

applied on the resonator at frequency $\omega_p = 2\tilde{\omega}_c$.

In deriving Eq. (5), it is worth mentioning that: (i) We have also assumed that the qutrit is initially in its ground state. As the qutrit-resonator system operates in the far-detuned dispersive regime, no energy is exchanged between the field mode (the resonator and the microwave field) and the qutrit, so the qutrit remains unexcited. Therefore, one can eliminate the degrees of freedom of the qutrit and the effective Hamiltonian is obtained. (ii) For a realistic implementation depicted in Fig. 1(b), we have ignored several terms due to their negligible effects, the highly off-resonance coupling between transitions (i.e., $|g\rangle \leftrightarrow |e\rangle$, $|e\rangle \leftrightarrow |f\rangle$) and the qutrit drives. For clarity, we have also omitted the term describing the coupling between the qutrit transition $|g\rangle \leftrightarrow |f\rangle$ and the resonator in the Hamiltonian in Eq. (1). However, this does not alter the main result except for making other contributions to the coefficients S and K; see Appendix A for the complete derivation. Moreover, these terms are taken into account in the following numerical analysis.

As a result, we have demonstrated that the qutrit-resonator system depicted in Fig. 1 can be modeled as a two-photon driven Kerr resonator. Recent theoretical studies have shown that the Schrödinger cat state can be generated via quantum adiabatic evolution of the system described by the Hamiltonian Eq. (5) [13,14]. This can be made clear by moving to a rotating frame with respect to $\omega_p a^\dagger a/2$ such that the Hamiltonian Eq. (5) is simplified to [14]

$$H = K a^{\dagger 2} a^2 - P(a^{\dagger 2} + a^2)$$

$$= K\left(a^{\dagger 2} - \frac{P}{K}\right)\left(a^2 - \frac{P}{K}\right) - \frac{P^2}{K}.$$ (9)

For simplicity, we assume that K and P are positive for the following discussion. It is apparent that the ground state is two-fold degenerate. The coherent states $|\pm\alpha\rangle$ ($\alpha = \sqrt{P/K}$) are the degenerate eigenstates with energy $-P^2/K$ and thus also the Schrödinger cat states

$$|\mathcal{C}_\alpha^\pm\rangle = \mathcal{N}_\alpha^\pm(|\alpha\rangle \pm |-\alpha\rangle), \quad \mathcal{N}_\alpha^\pm = \sqrt{2(1 \pm e^{-2\alpha^2})},$$ (10)

where $\mathcal{N}_\alpha^\pm$ is the normalizing factor; here the $\pm$ labels the even and odd cat states, respectively. Moreover, the
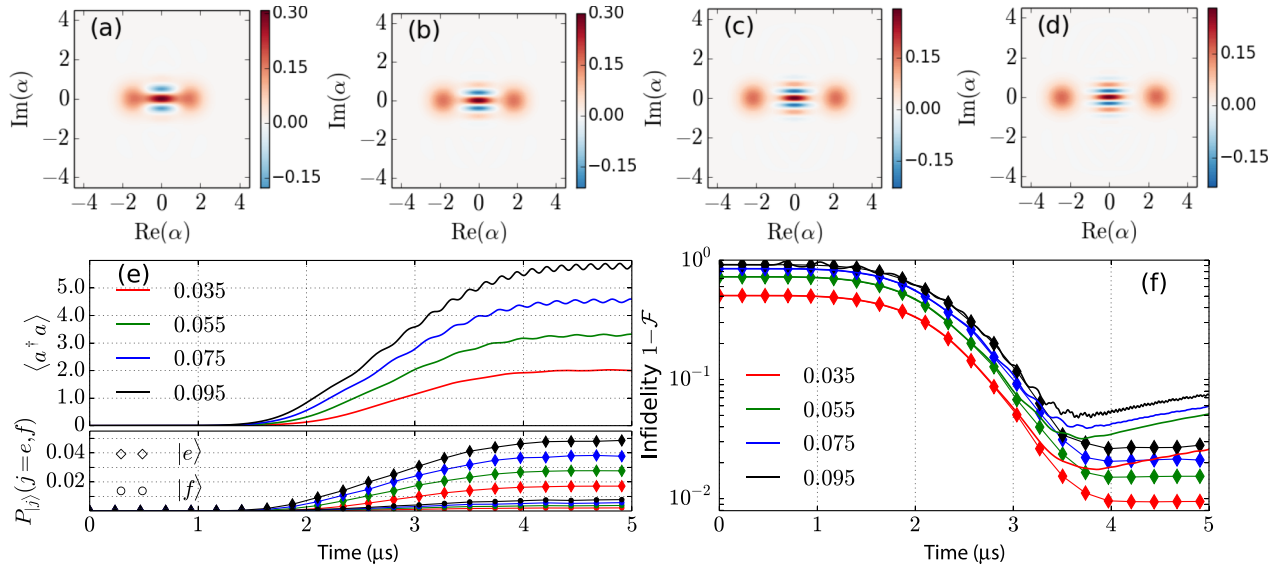
FIG. 2. Quantum adiabatic evolution of the system with a microwave drive $\Omega_p(t) = \Omega_p[1 - e^{-(t/\tau)^4}]$, where the system is initially in its ground state, i.e., the vacuum state $|0\rangle$ for the resonator and the $|g\rangle$ for the qutrit. The total time of the adiabatic evolution $T = 5~\mu s$ and $\tau = 3~\mu s$. (a), (b), (c), (d) The Wigner function for the resonator at the end of the adiabatic evolution for $\Omega_p/2\pi = (0.035, 0.055, 0.075, 0.095)$ GHz, respectively. (e) Time evolution of the average photon number $\langle a^\dagger a \rangle$ and population leakage to the excited state $(|e\rangle, |f\rangle)$ of the qutrit during the adiabatic evolution. (f) Time dependence of the fidelity of the cat state $\mathcal{F}(t)$. The parameters used in the numerical simulation are $\omega_c/2\pi = 5.25$ GHz, $\varepsilon_e/2\pi = 6.25$ GHz, $\varepsilon_f/2\pi = 10.0$ GHz, $g_{ge}/2\pi = 0.094$ GHz, $g_{ef}/2\pi = 0.136$ GHz, and $g_{gf}/2\pi = 0.140$ GHz. In (f), for the numerical simulation of the dynamics under the influence of dissipation, we use a decay rate of the resonator at $\kappa = 1/500$ MHz, and the decay rate of the qutrit with $\gamma_{ge} = \gamma_{gf} = 1/1.5$ MHz and $\gamma_{ef} = 1/1.0$ MHz.

vacuum state $|0\rangle$ and the one-photon Fock state $|1\rangle$ are also the ground eigenstates with even and odd parity for the undriven case ($P = 0$). As the Hamiltonian preserves the parity, when one gradually increases the amplitude of the two-photon drive $P(t)$, the driven system will evolve adiabatically along two paths $|\mathcal{C}_{\alpha_{(t)}}^{\pm}\rangle$ with $\alpha_{(t)} = \sqrt{P(t)/K}$ for the system initially prepared in the vacuum state and single-photon Fock state, respectively [13,14].

To show the validity of our proposal for the two-photon driven Kerr resonator, we present in Fig. 2 the numerical analysis of the time evolution of the qutrit-resonator system, initially in $|0, g\rangle$, with a microwave drive $\Omega_p(t) = \Omega_p[1 - e^{-(t/\tau)^4}]$ [14] applied on the qutrit (see Appendix B). The total evolution times T and τ are chosen to satisfy the adiabatic conditions and we use $T = 5~\mu s$ and $\tau = 3~\mu s$ in this work. The parameters used in the numerical simulation are $\omega_c/2\pi = 5.25$ GHz, $\varepsilon_e/2\pi = 6.25$ GHz, $\varepsilon_f/2\pi = 10.0$ GHz, $g_{ge}/2\pi = 0.094$ GHz, $g_{ef}/2\pi = 0.136$ GHz, and $g_{gf}/2\pi = 0.140$ GHz, yielding $K/2\pi \approx 0.450$ MHz. For the microwave drive with different amplitudes (i.e., $\Omega_p/2\pi = 0.035, 0.055, 0.075, 0.095$ GHz), Figs. 2(a)–2(d) show the Wigner function for the resonator at the end of the adiabatic evolution, respectively, and the resonator evolves to the even cat state $|\mathcal{C}_\alpha^+\rangle$ as we expected. The time evolution of the average photon number in the resonator is

also displayed in the upper panel of Fig. 2(e), and the photon number at time $t = T$ shows good agreement with the value calculated by P/K, yielding the average photon number $(2.08, 3.28, 4.47, 5.66)$ for the four different drive amplitudes, respectively.

The lower panel of Fig. 2(e) shows the population leakage to the excited state $(|e\rangle, |f\rangle)$ of the qutrit, where the diamond-marked line and circle-marked line represent the leakage to $|e\rangle$ and $|f\rangle$, respectively, which leads to an important limitation of our proposal for larger drive amplitudes. These results show that, for the fixed system parameter, increasing Ω_p will increase the population leakage, causing undesirable entanglement of the resonator and qutrit and adding another decay channel for the resonator. Figure 2(f) shows the time dependence of the fidelity of the cat state $\mathcal{F}(t) = \sqrt{\langle \mathcal{C}_\alpha^+ | \rho_r(t) | \mathcal{C}_\alpha^+ \rangle}$, in which $\alpha = \sqrt{P/K}$ and $\rho_r(t)$ is the reduced density matrix of the resonator. The marked line represents the time evolution of the fidelity without the effect of dissipation, while the solid line corresponds to the situation by considering the effect of photon decay and qutrit relaxation. As we expected, increasing the microwave drive amplitude will increase the infidelity. Meanwhile, the infidelity caused by this population leakage can be made smaller by increasing the qutrit-resonator detuning. However, we note that this increase would entail
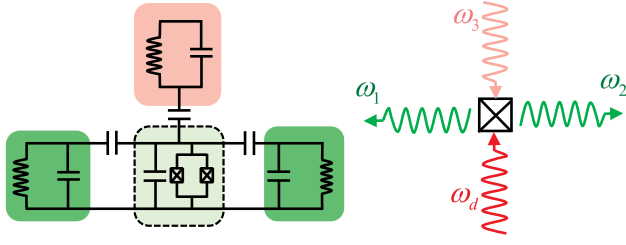
FIG. 3. Left panel: Circuit diagram of the system consisting of three resonators coupled to a superconducting transmon qubit, which can be used for implementation of the tunable resonant three-body interactions. Right panel: Diagrammatic representation of the mechanism behind the effective resonant three-body interactions: a four-wave mixing process in the nonlinear element, i.e., Josephson junction, induced by the pump at the frequency $\omega_d = \omega_1 + \omega_2 - \omega_3$, where a pump photon in combination with a resonator photon (with frequency ω_3) creates a photon in both the other two resonators at frequencies ω_1 and ω_2, respectively.

a sacrifice of the magnitude of the Kerr nonlinearity and the two-photon drive.

B. Tunable resonant interactions among three resonators

Here, we present a scheme for realizing a tunable three-resonator interaction and the interaction of interest to us is

$$H_{\text{three body}} = J_{123}(a_1^\dagger a_2^\dagger a_3 + a_1 a_2 a_3^\dagger), \qquad (11)$$

where $a_j^\dagger$ and a_j are the creation and annihilation operators, respectively, for the jth resonator of frequency ω_j. As shown in Fig. 3, we consider a system consisting of three strongly detuned resonators dispersively coupled to a transmon qubit. With the nonlinear cosine-coupling contribution from the Josephson junction of the transmon qubit, four-wave mixing processes that conserve energy can occur by applying a suitable pump mode on the qubit. Similar process have been experimentally demonstrated in 3D cQED architecture [30,47,48]. Here, we look for a four-wave mixing process where a pump photon in combination with a resonator photon (with frequency ω_3) can create a photon in both the other two resonators at frequencies ω_1 and ω_2, respectively, that results in the three-body interaction described by the interaction Hamiltonian given in Eq. (11).

Now, we give a quantitative derivation of the effective Hamiltonian. The Hamiltonian of the system depicted in Fig. 3 is [30]

$$H = \omega_q^{(0)} a_q^\dagger a_q + \sum_{j=1}^{3} \omega_j^{(0)} a_j^\dagger a_j - E_J \left(\cos\varphi + \frac{1}{2}\varphi^2 \right)$$
$$+ 2\varepsilon_p \cos(\omega_d t)(a_q^\dagger + a_q), \qquad (12)$$

where $a_m^\dagger$ and a_m ($m = q, 1, 2, 3$) are the creation and annihilation operators, respectively, for the mth mode with bare frequency $\omega_m^{(0)}$ and E_J is Josephson energy of the qubit mode. $\varphi = [\phi_q(a_q^\dagger + a_q) + \sum_{j=1}^{3} \phi_j(a_j^\dagger + a_j)]$ is the phase difference across the junction and ϕ_m ($m = q, 1, 2, 3$) is the zero-point fluctuation of the flux associated with the mth mode. The term in the second line of Eq. (12) describes a pump mode with real amplitude $2\varepsilon_p$ applied on the qubit mode at frequency ω_d.

In order to see clearly how the four-wave mixing process can lead to the desired three-resonator interaction, it is helpful to move to a displaced frame by performing a time-dependent transformation $U(t) = e^{-\tilde{\xi}_p a_q^\dagger + \tilde{\xi}_p^* a_q}$ with $\tilde{\xi}_p = \xi_p e^{-i\omega_d t}$ and $\xi_p = \varepsilon_p/(\omega_d - \omega_q)$ on the above Hamiltonian [30]. Assuming small phase fluctuations, we can expand the cosine up to the fourth order and the resulting Hamiltonian after a rotating-wave approximation in the displaced frame reads (see Appendix C for more details)

$$H = \sum_{j=1}^{3} \omega_j a_j^\dagger a_j + J_{123}(a_1^\dagger a_2^\dagger a_3 e^{-i\omega_d t} + a_1 a_2 a_3^\dagger e^{i\omega_d t}), \qquad (13)$$

where ω_j is the frequency for the jth mode including a renormalization of the transition frequency coming from the qubit-resonator coupling and the pump-mode-induced ac Stark shift. $J_{123} = -E_J \phi_1 \phi_2 \phi_3 \phi_q \xi_p$ is the three-body coupling strength, which can be controlled by the pump drive. When the pump frequency ω_d matches the detuning of the three resonators, i.e., $\omega_d = \omega_1 + \omega_2 - \omega_3$, the interaction Hamiltonian given in Eq. (11) is obtained. Moreover, by tuning the magnitude and the phase of the pump drive, one can realize an amplitude- and phase-tunable three-resonator interaction, which is useful to implement the ramp protocol for quantum annealing, as we demonstrate in the following section.

III. RESONATOR-BASED LECHNER-HAUKE-ZOLLER ANNEALER WITH THREE-BODY CONSTRAINTS

In this section, we show that our procedure to realize the two-photon driven Kerr resonator and the tunable resonance three-resonator interaction in the cQED architecture, as demonstrated in Sec. II, could be used for the implementation of quantum annealing with the LHZ scheme.

Here, for easy reference and to set the notation, we briefly review some basic concepts of quantum annealing and also the LHZ scheme. Quantum annealing was proposed as a quantum-enhanced optimizer that aims to efficiently solve optimization problems. In quantum annealing, one can map an optimization problem into the

all-to-all Ising spin-glass model [49]

$$H_P = \sum_{j=1}^{N} h_j \sigma_j^Z + \sum_{(j<k)} \mathcal{J}_{jk} \sigma_j^Z \sigma_k^Z, \qquad (14)$$

where σ_j^Z is the Pauli operator for the jth spin. The local field h_j and the strength of the spin-spin coupling $\mathcal{J}_{jk}$ fully define the optimization problem. The solution of the optimal problem now amounts to finding the ground state of the Ising spin-glass model (Ising problem) and this can be achieved by executing the time-dependent Hamiltonian

$$H(t) = \left(1 - \frac{t}{T}\right) H_I + \left(\frac{t}{T}\right) H_P, \qquad (15)$$

where H_I is the initial Hamiltonian with a trivial ground state (e.g., $H_I = \sum_{j=1}^{N} b_j \sigma_j^Z$) and T is the total evolution time. For a system that is governed by the Hamiltonian $H(t)$ and is initially in its ground state, evolving adiabatically, the system will stay in the instantaneous ground state of the Hamiltonian at each time t. Therefore, at the end of the evolution $t = T$, the system will stay in the ground state of H_P, which encodes the desired solution of the optimal problem.

However, to solve a practical optimal problem mapped into the Ising model with full connectivity, one leading physical restriction that makes the direct physical implementation of the model become untractable is that interactions between physical systems are commonly local, which favors local interactions between spins rather than long-range interactions. To get rid of this obstacle, an embedding technique, now known as the minor embedding scheme, was first introduced [50,51]. Recently, Lechner *et al.* [52] proposed an alternative embedding scheme in which the full connected Ising model with N logical spins [see Fig. 4(a)] is encoded in $N_P = N(N + 1)/2$ physical spins with $N_C = N(N - 1)/2$ local constraints in a triangular lattice, as shown in Fig. 4(b) [53]. In the LHZ scheme, each physical spin encodes the relative orientation of the corresponding pair of logical spins, i.e., the physical spins take $|\uparrow\rangle$ and $|\downarrow\rangle$ for the aligned (i.e., $|\uparrow\uparrow\rangle$, $|\downarrow\downarrow\rangle$) and antialigned (i.e., $|\uparrow\downarrow\rangle$, $|\downarrow\uparrow\rangle$) logical pair, respectively. Meanwhile, local constraints are introduced to suppress the redundancy of the encoding scheme. With this scheme, only local four-body terms and programmable local fields applied on the physical spin are needed [54]. These features along with the potential of scaling up make it attractive for practical physical implementations, and various physical implementation schemes have been proposed [22,55–57] and demonstrated experimentally for small systems [58]. In particular, the resonator-based implementation proposed in Ref. [22] has been shown to be realizable and noise resilient. Therefore, in the following discussion, by combining the advantage of this resonator-based implementation and the long coherence times attainable in 3D
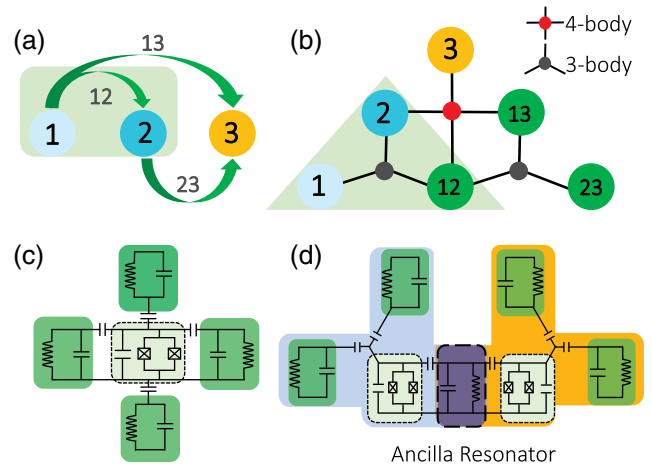

FIG. 4. Illustration of the fully connected architecture with three-body constraints. (a) Graph of the fully connected Ising problem with $N = 3$ logical qubits. (b) LHZ implementation of the same problem with $N_p = N(N + 1)/2 = 6$ physical qubits and $N_C = N(N - 1)/2 = 3$ local constraints. (c) Circuit-QED architecture for the physical implementation of the four-body constraints needed in the Kerr-resonator-based LHZ scheme. (d) Decomposition of the four-body constraints into two three-body constraints by using an ancillary resonator.

cQED, we propose a scalable hardware for implementing a resonator-based LHZ annealer with three-body constraints, which is compatible with the 3D cQED architecture.

A. The Lechner-Hauke-Zoller scheme with three-body constraints

In the LHZ scheme, each four-body constraint can be realized directly by using a four-spin interaction $\sigma_{l,n}^Z \sigma_{l,s}^Z \sigma_{l,e}^Z \sigma_{l,w}^Z$, in which (l,n), (l,s), (l,e), and (l,w) label the physical spin involved in the lth four-body constraint and the interaction strength should be the dominant energy scale in the embedding model [52,56]. Therefore, for a physical implementation of the LHZ scheme with four-body constraints, the Ising-problem Hamiltonian reads [52]

$$H_P^{\text{LHZ4}} = \sum_{j=1}^{N_P} h_j \sigma_j^Z - C \sum_{l=1}^{N_C} \sigma_{l,n}^Z \sigma_{l,s}^Z \sigma_{l,e}^Z \sigma_{l,w}^Z, \qquad (16)$$

with logical field h_j acting on the jth physical spin and C the magnitude of the four-spin coupling strength.

However, the four-spin interaction is still hard to physically realize with considerably high coupling strength. Recently, Leib *et al.* [55] have theoretically demonstrated that one can use a general recursive decomposition of classical k-local Ising terms, decomposing the four-body constraints into two three-body constraints,

$$\sigma_{l,n}^Z \sigma_{l,s}^Z \sigma_{l,e}^Z \sigma_{l,w}^Z \rightarrow \sigma_{l,n}^Z \sigma_{l,w}^Z \sigma_{l,a}^Z + \sigma_{l,a}^Z \sigma_{l,s}^Z \sigma_{l,e}^Z, \qquad (17)$$

with an ancillary physical spin denoted by (l, a). It is noted here that each ancillary physical spin does not encode any information of the logical spin configuration, but rather mediates the three-body realization of the four-body constraints. Therefore, one can realize the LHZ scheme with three-body constraints, which can be realized directly by using a three-body interaction $\sigma_i^Z \sigma_j^Z \sigma_k^Z$. For a physical implementation of the LHZ scheme with three-body constraints, the Ising-problem Hamiltonian becomes

$$H_P^{\text{LHZ}_3} = \sum_{j=1}^{\tilde{N}_P} h_j \sigma_j^Z - C \sum_{l=1}^{\tilde{N}_C} \sigma_{l,i}^Z \sigma_{l,j}^Z \sigma_{l,k}^Z, \qquad (18)$$

with $\tilde{N}_P = N(N-1) + 1$ and $\tilde{N}_C = (N-1)^2$.

In order to evaluate the performance of the LHZ scheme with three-spin interactions, we present in Fig. 5 the time-dependent energy spectrum of the executing Hamiltonian for the Ising problem with $N = 3$ logical spins; the Ising-problem Hamiltonians are represented by Eqs. (14), (16), and (18). In the numerical simulation, we consider that the initial Hamiltonian is given as $H_I = \sum_{j=1}^N b_j \sigma_j^Z$ with $b_j = \mathcal{J}$, and we use the local field strength h_j, spin-spin coupling strength $\mathcal{J}_{jk}$ that is randomly taking from the interval $[-\mathcal{J}, \mathcal{J}]$, and the constraint strength $C/\mathcal{J} = 3$. As shown in Fig. 5, although different trajectories of the time-dependent spectrum have been shown for the three schemes, an almost perfect agreement of the lower 2^3 energy levels is displayed at time $t = T$, demonstrating preliminarily the validity of the three-body constraint implementation of the Ising problem.
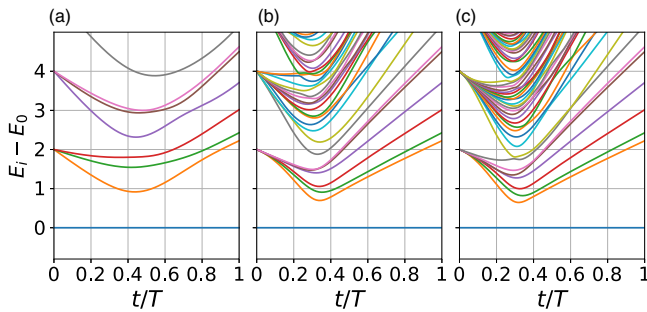

FIG. 5. Time-dependent spectrum of an annealing process for the Ising problem with $N = 3$ logical spins. The values of parameter used in numerical simulation are: the local field acting on the jth logical spin h_j and the spin-spin coupling strength $\mathcal{J}_{jk}$ are random numbers taken from the interval $[-\mathcal{J}, \mathcal{J}]$. (a) Fictitious direct implementation. (b) Implementation with the LHZ scheme, where each four-body constraint is realized directly by using a four-spin interaction. (c) Implementation with the LHZ scheme where each four-body constraint is represented by two three-body constraints that are physically realized by using three-spin interactions. Here, t is the time, T is the total evolution time, and E_i is the eigenenergy. We use a constraint strength $C/\mathcal{J} = 3$.
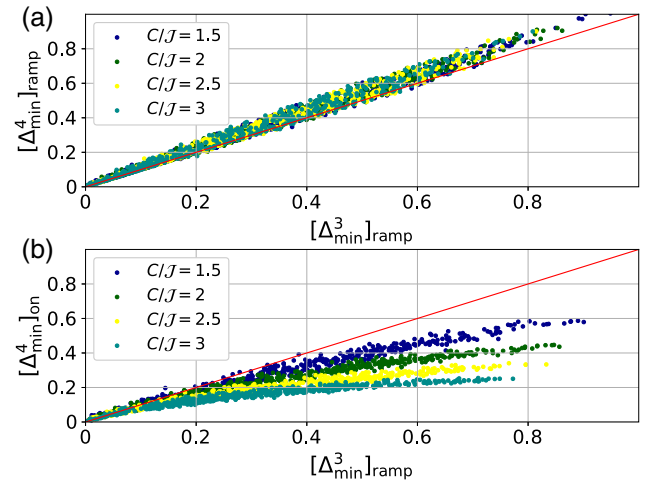

FIG. 6. Scatter plot showing the minimal gap in the annealing process for the LHZ scheme with three-spin interaction Δ_{min}^3 versus the minimal gap with four-spin interaction Δ_{min}^4. The points (belonging to the same color) correspond to 500 random instances with a given constraint strength. The constraint strengths are $C/\mathcal{J} = (1.5, 2, 2.5, 3)$ and the parameters of the Ising problem used are the same as that in Fig. 5. (a) For both LHZ implementations, we use a ramp protocol, i.e., $[\Delta_{\text{min}}^3]_{\text{ramp}}$ versus $[\Delta_{\text{min}}^4]_{\text{ramp}}$. (b) The ramp protocol for the three-spin interaction implementation $[\Delta_{\text{min}}^3]_{\text{ramp}}$ against the always-on protocol for the four-spin interaction implementation $[\Delta_{\text{min}}^4]_{\text{on}}$.

In the practical quantum annealing process, the minimal gap is the leading limitation restricting the sweep time and also the main source of errors in quantum annealing, i.e., Landau-Zener transitions. For the LHZ scheme with three-body and four-body constraints, we further present in Fig. 6(a) the comparison of the minimal gap. For 500 random instances, the three-body-constraint-based implementation does not considerably decrease the minimal gap and even the two implementations show a similar result for four different constraint strengths ($C/\mathcal{J} = 1.5, 2, 2.5, 3$).

Alternatively, compared with the ramp protocol described by the Hamiltonian Eq. (15), where in the annealing process the constraint terms are adiabatically changed form 0 to C, it is also possible to use an always-on protocol (i.e., the strengths of the constraints are fixed in the whole process). Using this always-on protocol, the Ising problem encoded by the LHZ scheme is fully characterized by the local fields applied on the physical spin, and thus one can simplify the physical system and reduce the complexity for quantum annealing. Recent theoretical studies have demonstrated that the gap in the always-on protocol is in general smaller, but with only a small systematic difference between the two in favor of the ramp protocol [55]. However, as shown in Fig. 6(b), the minimal gap in the three-body implementation with ramp protocol $[\Delta_{\text{min}}^3]_{\text{ramp}}$ is generally larger than the one in the four-body

always-on protocol $[\Delta^4_{\min}]_{\text{on}}$. This suggests that the three-body implementation with ramp protocol may have better performance than the four-body always-on protocol. In the following discussion, we propose a resonator-based system for implementing the LHZ scheme with three-body constraints, where the tunable three-body interactions in the proposed system allow for the ramp protocol.

B. The coupled network with application to the Lechner-Hauke-Zoller annealer

Here we show that the cQED architecture proposed in Sec. II. can be used for implementing the LHZ annealer with three-body constraints as introduced in Sec. III A. Following the recent theoretical studies in Ref. [22], in our setting the spin states $\{|\uparrow\rangle, |\downarrow\rangle\}$ are encoded in the degenerate ground subspace of the two-photon driven Kerr resonator formed by two coherent states of opposite phases, i.e., $\{|\alpha\rangle, |-\alpha\rangle\}$, respectively, and the three-body constraints are directly implemented with three-resonator interactions mediated by the transmon qubit. Moreover, as demonstrated in Sec. II B, the strength of the three-resonator interaction can be easily tuned by varying the microwave fields acting on the transmon qubit, thus making it particularly appealing for the implementation of the LHZ annealer with ramp protocol.

In order to realize the spin lattice with triangular structures required for implementing the LHZ annealer [see Fig. 4(b)], we consider that each spin is physically realized by a two-photon driven Kerr resonator and all the four-body constraints are implemented by two three-body constraints with an ancillary resonator [see Figs. 4(c) and 4(d)]; thus all the three-body constraints (including both the three-body constraints in the base of the lattice and the required three-body constraints used for realizing four-body constraints) can be directly implemented by using the qubit-mediated three-resonator interactions as introduced in Sec. II B. Meanwhile, the local field acting on each spin is implemented by introducing a single-photon drive applied on the resonator [21,22]. To implement the adiabatic ramp protocol for the LHZ annealer with three-body interactions [see Eq. (18)] in our proposed architecture, the executing time-dependent Hamiltonian reads (in the laboratory frame)

$$H_N^{\text{LHZ}}(t) = \sum_{j=1}^{\tilde{N}_P} (H_j + H_j^{(d)}) + \sum_{(i,j,k)\in l}^{\tilde{N}_C} H_{ijk}^C. \quad (19)$$

In the above equation,

$$H_j = \omega_j a_j^\dagger a_j + K_j a_j^{\dagger 2} a_j^2$$
$$- \varepsilon_j^{(p)}(t)(a_j^{\dagger 2} e^{-i\omega_j^{(p)}(t)t} + a_j^2 e^{i\omega_j^{(p)}(t)t}) \quad (20)$$
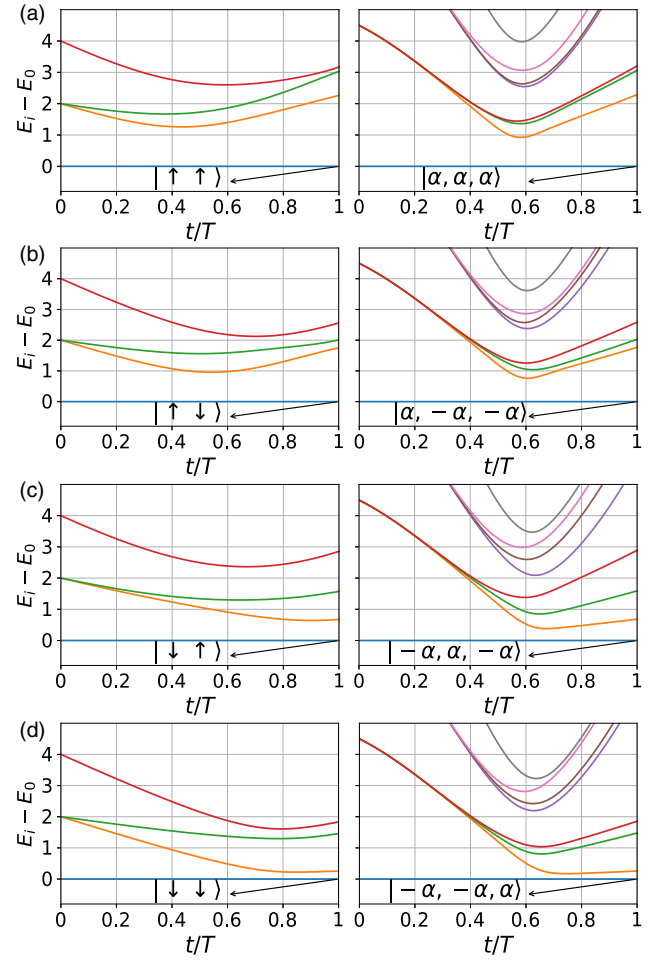

FIG. 7. Time-dependent spectrum. Left panels: The energy spectrum during adiabatic evolution for the Ising problem with $N = 2$ logical spins, represented by shallow green blocks in Fig. 4(a). Right panels: resonator-based LHZ scheme with three-body constraints described by Eq. (27), represented by shallow green blocks in Fig. 4(b). The parameters of the Ising problem used are the same as that of Fig. 5 and we use the constraint strength $C/\mathcal{J} = 3$. Resonator system parameters for the calculation are $\delta_1/\mathcal{J} = \delta_2/\mathcal{J} = \delta_3/\mathcal{J} = 4.5$, $K_j/\mathcal{J} = 10$, and $\varepsilon_j^{(p)}/\mathcal{J} = 20$, resulting in $\alpha = \sqrt{\varepsilon_j^{(p)}/K_j} = \sqrt{2}$, and $J_{123}/\mathcal{J} \approx -0.53$. In the left panels of (a)–(d), the arrowed lines mark the spin configuration of the ground state at time $t = T$, i.e., $\{|\uparrow\uparrow\rangle, |\uparrow\downarrow\rangle, |\downarrow\uparrow\rangle, |\downarrow\downarrow\rangle\}$, respectively, and in the right panels, the state of the first two resonators reproduces the spin configuration of the ground state of the Ising problem, while the state of the third resonator confirms the relative orientation of the two logical spins.

describes the jth two-photon driven resonator with self-Kerr coefficient K_j and time-dependent two-photon driving of amplitude $\varepsilon_j^{(p)}(t) = \varepsilon_j^{(p)} t/T$ at frequency $\omega_j^{(p)}(t)$ that can be realized in the cQED architecture introduced in Sec. II A.

$$H_j^{(d)} = \varepsilon_j^{(d)}(t)(a_j^\dagger e^{-i\omega_j^{(d)}(t)t} + a_j e^{i\omega_j^{(d)}(t)t}), \quad (21)$$

represents the additional time-dependent single-photon driving of amplitude $\varepsilon_j^{(d)}(t) = \varepsilon_j^{(d)} t/T$ applied on the jth resonator at frequency $\omega_j^{(d)}(t) = \omega_j^{(p)}(t)/2 = \omega_j - \delta_j(t)$, in which $\delta_j(t) = \delta_j(1 - t/2T)$ is the detuning of the resonator relative to the single-photon driving frequency. This single-photon driving is introduced as the local field acting on the spin defined in the subspace of the corresponding resonator and, to see more clearly, by moving into a frame rotating at this single-photon driving frequency via the unitary transformation $U = e^{-i\omega_j^{(d)}(t) t a_j^\dagger a_j}$, and by projecting this driving Hamiltonian onto the encoding space $\Pi = \Pi_{|\alpha\rangle} + \Pi_{|-\alpha\rangle}$ defined by $\{\Pi_{|\pm\alpha\rangle} = |\pm\alpha\rangle\langle\pm\alpha|\}$, one can obtain the effective Hamiltonian (note that α is a positive number in our setting)

$$\varepsilon_j^{(d)}(t)\Pi(a_j^\dagger + a_j)\Pi = 2\alpha\varepsilon_j^{(d)}(t)\sigma_j^Z, \qquad (22)$$

where $\sigma_j^Z = \Pi_{|\alpha\rangle} - \Pi_{|-\alpha\rangle}$. Indeed, this single-photon driving can serve as the local field acting on the jth spin that is defined in the encoding subspace Π.

$$H_{ijk}^C = J_{ijk}(t)(a_i^\dagger a_j^\dagger a_k e^{-i\omega_d^{(l)} t} + a_i a_j a_k^\dagger e^{i\omega_d^{(l)} t}), \qquad (23)$$

denotes the three-resonator interaction with strength $J_{ijk}(t) = J_{ijk}t/T$, which is induced by a pump mode at frequency $\omega_d^{(l)} = [\omega_i^{(d)}(t) + \omega_j^{(d)}(t) - \omega_k^{(d)}(t)]_{(i,j,k)\in l}$ applied on the ancillary Transmon qubit as demonstrated in Sec. II B. Once again, by moving into the rotating frame with single-photon drives, and after projecting this three-resonator interaction Hamiltonian onto the tensor product of the encoding space (i.e., $\Pi_3 = \Pi^{\otimes 3}$), one can obtain the effective Hamiltonian

$$J_{ijk}(t)\Pi_3(a_i^\dagger a_j^\dagger a_k + a_i a_j a_k^\dagger)\Pi_3 = 2\alpha^3 J_{ijk}(t)\sigma_i^Z\sigma_j^Z\sigma_k^Z \quad (24)$$

thus this three-resonator interaction can be used to implement the three-body constraints needed to execute the proposed LHZ annealer [see Eq. (18)].

According to the above observations and considerations, by having both single-photon driving and the three-resonator interactions, one can realize the two ingredients for implementing the LHZ annealer with three-body constraints. Following the same procedure as that used in the above discussions, by moving into a frame where each of the resonators rotates at the instantaneous single-photon drive frequency, i.e., applying the unitary transformation

$$U = e^{-i\sum_{j=1}^{\tilde{N}_P} \omega_j^{(d)}(t) t a_j^\dagger a_j}, \qquad (25)$$

on the executing Hamiltonian for the LHZ annealer $H_N^{\text{LHZ}}(t)$ given in Eq. (19),

$$\tilde{H}_N^{\text{LHZ}}(t) = U(t)^\dagger H_N^{\text{LHZ}}(t)U(t) - iU(t)^\dagger \dot{U}(t), \qquad (26)$$

one can rewrite the executing Hamiltonian as [22]

$$\tilde{H}_N^{\text{LHZ}}(t) = \left(1 - \frac{t}{T}\right)H_I + \left(\frac{t}{T}\right)H_P^{\text{LHZ}_R}, \qquad (27)$$

where

$$H_I = \sum_{j=1}^{\tilde{N}_P}[(\delta_j a_j^\dagger a_j + K_j a_j^{\dagger 2} a_j^2), \qquad (28)$$

acts as the initial Hamiltonian whose ground state is a rather trivial state. This is especially true in this case, since each of the resonators is just in the vacuum state, which is actually simpler to prepare with state-of-the-art technology.

$$H_P^{\text{LHZ}_R} = \sum_{j=1}^{\tilde{N}_P}[K_j a_j^{\dagger 2} a_j^2 + \varepsilon_j^{(p)}(a_j^{\dagger 2} + a_j^2) + \varepsilon_j^{(d)}(a_j^\dagger + a_j)]$$

$$+ \sum_{(i,j,k)\in l}^{\tilde{N}_C} J_{ijk}(a_i^\dagger a_j^\dagger a_k + a_i a_j a_k^\dagger), \qquad (29)$$

characterizes the Ising problem by using the LHZ scheme with three-body constraints. The correspondence between the above equation and the problem Hamiltonian $H_P^{\text{LHZ}_3}$ [see Eq. (18)] can be found directly by projecting Eq. (29) onto the tensor product of the encoding apace (i.e., $\Pi_{\tilde{N}_P} = \Pi^{\otimes \tilde{N}_P}$). Therefore, according to Eqs. (22) and (24), and by dropping constant terms, the effective Hamiltonian in the rotating frame projected onto the encoding space reads

$$H_P^{\text{LHZ}_R} = \sum_{j=1}^{\tilde{N}_P} h_j\sigma_j^Z + \sum_{(i,j,k)\in l}^{\tilde{N}_C} C_{ijk}\sigma_{l,i}^Z\sigma_{l,j}^Z\sigma_{l,k}^Z, \qquad (30)$$

with $h_j = 2\varepsilon_j^{(d)}\alpha$ and $C_{ijk} = 2J_{ijk}\alpha^3$. It is clear from the above observations that the Ising-problem Hamiltonian given in Eq. (18) can be implemented in the proposed coupled network. However, as mentioned in Ref. [59] and demonstrated in Refs. [14,22], the validity of the proposed implementation is maintained only if the single-photon-drive strength $\varepsilon_j^{(d)}$ is sufficiently small and also the three-resonator coupling strength J_{ijk}.

To give a preliminary verification of the above resonator-based LHZ annealer, we present in Fig. 7 the time-dependent energy spectrum of the Hamiltonian in Eqs. (15) and (27), with $N = 2$. At the end of the evolution $t = T$, an almost perfect agreement of the lower 2^N energy levels is displayed and thus, in principle, by executing the resonator-based LHZ annealer one can indeed find the correct ground state for a given Ising problem described by Eq. (14). Furthermore, in the left panel of Fig. 7, we present the spin configuration of the ground state of the Ising

problem described by Eq. (15) with different parameters, resulting in $\{|\uparrow\uparrow\rangle, |\uparrow\downarrow\rangle, |\downarrow\uparrow\rangle, |\downarrow\downarrow\rangle\}$ for Figs. 7(a)–7(d), respectively. We also show, in the right panel, the ground state of the corresponding resonator-based LHZ annealer at time $t = T$, where the state of the first two resonators reproduces the spin configuration of the ground state of the Ising problem, while the state of the third resonator confirms the relative orientation of the two logical spins. The whole fidelities $\mathcal{F} = \langle s_1\alpha, s_2\alpha, s_3\alpha|\Psi_0(T)\rangle$, in which $\alpha = \sqrt{\varepsilon_j^{(p)}/K_j} = \sqrt{2}$, $s_i = \pm$ $(i = 1, 2, 3)$ is the sign of the amplitude of the ith resonator for an ideal encoding, and $|\Psi_0(T)\rangle$ is the eigenstate of the executing Hamiltonian given in Eq. (27) at $t = T$, are 99.93%, 99.93%, 99.93%, and 99.94% for the four different spin configurations, respectively, demonstrating preliminarily the reliability of the proposed resonator-based LHZ annealer.

IV. CONCLUSION

In conclusion, we propose a realizable scheme for implementing a two-photon driven Kerr resonator in a cQED architecture consisting of a superconducting resonator capacitively coupled to a microwave-driven superconducting qubit and, by using realistic parameters, we show that the Schrödinger cat state can be prepared via adiabatic evolution in the microwave-driven qubit-resonator system. Contrary to the implementation by using a superconducting coplanar resonator terminated by a flux-pumped SQUID, our protocol is compatible with the 3D architecture that allows us to exploit the large coherence times of the 3D microwave superconducting resonator. The major limitation of our proposal is the population leakage for lager drive amplitudes, which results in infidelity, and in principle, this can be further decreased by looking for an optimal parameter set of the qubit-resonator system. As a possible extension, one may also apply this protocol to a hybrid quantum system consisting of a spin or atomic ensemble coupled to superconducting circuits [60], allowing generation of a spin (atomic) Schrödinger cat state and spin squeezing for quantum-enhanced sensing and metrology [61,62].

Inspired by recent theoretical work, we further show that the presented architecture to realize a two-photon driven Kerr resonator together with the introduced tunable three-resonator interaction can be easily scaled up to a coupled network for the implementation of a resonator-based LHZ annealer. The tunable three-resonator interaction allows for the ramp protocol of our quantum annealer. Therefore, comparing with the always-on protocol, our implementation with ramp protocol may have better performance. Furthermore, in principle, the annealer that we have proposed can be realized in the 3D cQED architecture [63,64], for which the coherence times of the 3D microwave superconducting resonator can exceed that of the best superconducting qubit (or superconducting coplanar resonator) by almost two orders of magnitude [38,39]. This makes our proposed implementation a promising physical platform for realizing a quantum annealer with improved coherence.

APPENDIX A: THE REALISTIC CIRCUIT-QED IMPLEMENTATION

Figure 8 shows the circuit model of the capacitively shunted flux qubit (C-shunt flux qubit) [67,68], which is capacitively coupled to an LC resonator [68–70]. The two identical Josephson junctions have capacitance C_J and coupling energy E_J, while the third (smaller one) has capacitance αC_J and coupling energy αE_J. L_r and C_r represent the equivalent inductance and capacitance of the resonator, respectively. C_c represents the coupling capacitance between the resonator and the flux qubit, for which the smaller junction is shunted by a capacitance C_{sh}. In the following discussion, the phase difference across the larger Josephson junctions and the inductance L_r are denoted by φ_i $(i = 1, 2)$ and φ_r, respectively. The Lagrangian of the system is given by

$$\mathcal{L} = \frac{C_J}{2}\left(\frac{\Phi_0}{2\pi}\right)^2 \dot{\varphi}_1^2 + \frac{C_J}{2}\left(\frac{\Phi_0}{2\pi}\right)^2 \dot{\varphi}_2^2$$
$$+ \frac{\alpha C_J}{2}\left(\frac{\Phi_0}{2\pi}\right)^2 (\dot{\varphi}_1 - \dot{\varphi}_2)^2$$
$$+ \frac{C_{sh}}{2}\left(\frac{\Phi_0}{2\pi}\right)^2 (\dot{\varphi}_1 - \dot{\varphi}_2)^2 + U$$
$$+ \frac{C_c}{2}\left(\frac{\Phi_0}{2\pi}\right)^2 (\dot{\varphi}_r + \dot{\varphi}_1 - \dot{\varphi}_2)^2$$
$$+ \frac{C_r}{2}\left(\frac{\Phi_0}{2\pi}\right)^2 \dot{\varphi}_r^2 - \frac{1}{2L_r}\left(\frac{\Phi_0}{2\pi}\right)^2 \varphi_r^2, \quad \text{(A1)}$$

where Φ_0 is the magnetic flux quantum, and $U = E_J\cos\varphi_1 + E_J\cos\varphi_2 + \alpha E_J\cos(\varphi_1 - \varphi_2 + 2\pi f)$ with $f = \Phi_e/\Phi_0$, where Φ_e is the externally applied magnetic flux in the loop. For clarity, this equation can be rewritten
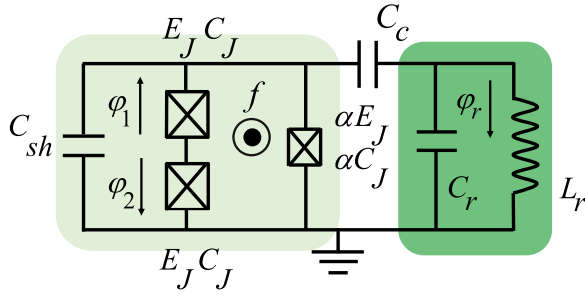
FIG. 8. Circuit model of the capacitively shunted flux qubit (C-shunt flux qubit) capacitively coupled to an LC resonator.

as

$$\mathcal{L} = \frac{C_J}{2}\left(\frac{\Phi_0}{2\pi}\right)^2 \dot{\varphi}_1^2 + \frac{C_J}{2}\left(\frac{\Phi_0}{2\pi}\right)^2 \dot{\varphi}_2^2$$

$$+ \frac{\alpha' C_J}{2}\left(\frac{\Phi_0}{2\pi}\right)^2 (\dot{\varphi}_1 - \dot{\varphi}_2)^2$$

$$+ U + \frac{C_c}{2}\left(\frac{\Phi_0}{2\pi}\right)^2 (\dot{\varphi}_r + \dot{\varphi}_1 - \dot{\varphi}_2)^2$$

$$+ \frac{C_r}{2}\left(\frac{\Phi_0}{2\pi}\right)^2 \dot{\varphi}_r^2 - \frac{1}{2L_r}\left(\frac{\Phi_0}{2\pi}\right)^2 \varphi_r^2, \quad (A2)$$

with $\alpha' = \alpha + C_{\rm sh}/C_J$. Following the procedure of Ref. [70], the system can described by a Hamiltonian consisting of three parts:

$$H_{qr} = H_q + H_r + H_c, \quad (A3)$$

where

$$H_q = 4E_c \frac{(1+\alpha')(1+\gamma) + \beta}{(1+2\alpha')(1+\gamma) + 2\beta}(n_1^2 + n_2^2)$$

$$+ 8E_c \frac{\alpha'(1+\gamma) + \beta}{(1+2\alpha')(1+\gamma) + 2\beta}n_1 n_2 - U \quad (A4)$$

is the qubit Hamiltonian,

$$H_r = \omega_c a^\dagger a \quad (A5)$$

is the resonator Hamiltonian, and

$$H_c = \frac{-2i}{(1+2\alpha'+2\beta)^{1/4}}\sqrt{\frac{\beta\gamma}{[(1+2\alpha')(1+\gamma)+2\beta]^{3/2}}}$$

$$\times \sqrt{E_r E_c}(n_1 - n_2)(a^\dagger - a), \quad (A6)$$

is the qubit-resonator interaction Hamiltonian. Above, $a^\dagger$ and a are the creation and annihilation operators, respectively, for the resonator with frequency

$$\omega_c = \frac{1}{\sqrt{L_r C_r}}\sqrt{\frac{1+2\alpha'+2\beta}{(1+2\alpha')(1+\gamma)+2\beta}}, \quad (A7)$$

TABLE I. Component parameters of the qubit-resonator system used for the energy level and coupling strength calculations in Fig. 9.

C_J	10.76 fF
$E_J/2\pi$	135.00 GHz
α	0.60
$C_{\rm sh}$	22.06 fF
C_c	5.92 fF
$E_r/2\pi$	5.25 GHz

and $E_r = 1/\sqrt{L_r C_r}$, $E_c = e^2/2C_J$, $\beta = C_c/C_J$, $\gamma = C_c/C_r$, and n_i ($i = 1, 2$) are conjugate variables of the phase differences φ_i.

According to the parameters listed in Table I, Figure 9 shows the energy spectrum of the flux qubit from the ground state and the coupling strength,

$$g_{ij} = \left|\frac{-2i}{(1+2\alpha'+2\beta)^{1/4}}\sqrt{\frac{\beta\gamma}{[(1+2\alpha')(1+\gamma)+2\beta]^{3/2}}}\right.$$

$$\left.\times \sqrt{E_r E_c}\langle i|(n_1 - n_2)|j\rangle\right|, \quad (A8)$$

where $|j\rangle$ represents the jth eigenstate of the uncoupled qubit Hamiltonian given in Eq. (A4), as a function of the flux bias f.

In this work, we focus on the lowest three energy levels of the flux qubit and thus in this situation the flux qubit is considered to be a perfect three-level system (qutrit). After
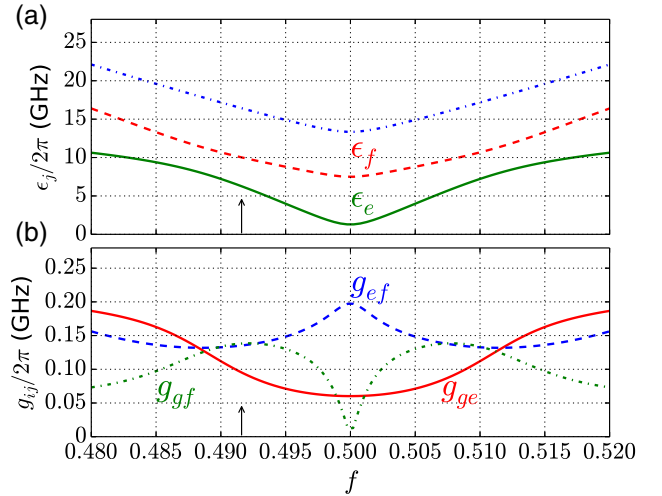
FIG. 9. (a) The energy spectrum of the flux qubit from the ground state. (b) The coupling strength $g_{ij} = |\langle i|H_c|j\rangle|$. In this work, the biased point of interest to us is indicated by the vertical arrow, i.e., $f = 0.4916$. This results in the system parameters used for numerical analysis in the main text, $\varepsilon_e/2\pi = 6.25$ GHz, $\varepsilon_f/2\pi = 10.0$ GHz, $g_{ge}/2\pi = 0.094$ GHz, $g_{ef}/2\pi = 0.136$ GHz, and $g_{gf}/2\pi = 0.140$ GHz.

using the RWA, the Hamiltonian of the qutrit-resonator system is

$$
\begin{aligned}
H_{q_r} &= \omega_c a^\dagger a + \sum_{j=g,e,f} \epsilon_j |j\rangle\langle j| + H_c, \\
H_c &= g_{ge}|g\rangle\langle e|a^\dagger + g_{ef}|e\rangle\langle f|a^\dagger + g_{gf}|g\rangle\langle f|a^\dagger + \text{H.c.}
\end{aligned}
\tag{A9}
$$

By introducing a microwave drive tone applied on the qutrit, the full-system Hamiltonian reads

$$
H_{\text{full}} = H_{q_r} + H_d, \tag{A10}
$$

where

$$
\begin{aligned}
H_d &= \Omega_{ge}^{(p)} e^{-i\omega_p t}|e\rangle\langle g| + \Omega_{ef}^{(p)} e^{-i\omega_p t}|f\rangle\langle e| \\
&\quad + \Omega_{gf}^{(p)} e^{-i\omega_p t}|f\rangle\langle g| + \text{H.c.},
\end{aligned}
\tag{A11}
$$

where H.c. stands for Hermitian conjugate and ϵ_j ($j = g, e, f$) is the transition frequency of the qutrit from ground to excited state $|j\rangle$. g_{ge}, g_{ef}, and g_{gf} denote the qutrit-resonator coupling strengths. $\Omega_{jk}^{(p)}$ is the real amplitude of the microwave drive with frequency ω_p applied to the $|j\rangle \longleftrightarrow |k\rangle$ transition of the qutrit. For simplicity, we define $\epsilon_g = 0$ in the following discussion.

We consider that our system operates in the dispersive regime, where the qutrit is detuned from the resonator $|\Delta_{jk}| = |(\epsilon_j - \epsilon_k) - \omega_c| \gg g_{jk}$ and the qutrit is off-resonantly driven by the microwave drive $|\Delta'_{jk}| = |(\epsilon_j - \epsilon_k) - \omega_p| \gg \Omega_{jk}^{(p)}$. Moreover, we suppose that the qutrit is initially in its ground state. Therefore, the qutrit remains unexcited in the process and thus decouples from the resonator. In these conditions, by using fourth-order perturbation theory [44,71] and eliminating the degrees of freedom of the qutrit, the Hamiltonian in Eq. (A10) can be well approximated by the effective Hamiltonian

$$
H_{\text{eff}} = \tilde{\omega}_c a^\dagger a + K a^{\dagger 2} a^2 - P(a^{\dagger 2} e^{-i\omega_p t} + \text{H.c.}), \tag{A12}
$$

where $\tilde{\omega}_c = \omega_c + S$ is the dressed resonator frequency with

$$
\begin{aligned}
S &= -\frac{g_{ge}^2}{\omega_e - \omega_c} - \frac{g_{gf}^2}{\omega_f - \omega_c} + \frac{g_{ge}^4}{(\omega_e - \omega_c)^3} \\
&\quad + \frac{g_{gf}^4}{(\omega_f - \omega_c)^3} + \frac{g_{gf}^2 g_{ef}^2}{(\omega_c - \omega_f)(-\omega_e)(\omega_c - \omega_f)} \\
&\quad - \frac{g_{ge}^2 g_{gf}^2}{(\omega_c - \omega_e)^2(\omega_c - \omega_f)} - \frac{g_{ge}^2 g_{gf}^2}{(\omega_c - \omega_e)(\omega_c - \omega_f)^2}.
\end{aligned}
\tag{A13}
$$

The second term denotes the qutrit-induced Kerr nonlinearity of the resonator with

$$
\begin{aligned}
K &= \frac{g_{ge}^4}{(\omega_e - \omega_c)^3} + \frac{g_{gf}^4}{(\omega_f - \omega_c)^3} \\
&\quad + \frac{g_{ge}^2 g_{ef}^2}{(\omega_c - \omega_e)(2\omega_c - \omega_f)(\omega_c - \omega_e)} \\
&\quad + \frac{g_{gf}^2 g_{ef}^2}{(\omega_c - \omega_f)(-\omega_e)(\omega_c - \omega_f)} \\
&\quad - \frac{g_{ge}^2 g_{gf}^2}{(\omega_c - \omega_e)^2(\omega_c - \omega_f)} - \frac{g_{ge}^2 g_{gf}^2}{(\omega_c - \omega_e)(\omega_c - \omega_f)^2}.
\end{aligned}
\tag{A14}
$$

The last term represents a two-photon drive of amplitude

$$
P = -\frac{g_{ge} g_{ef} \, \Omega_{gf}^{(p)}}{\Delta_{ge}(\epsilon_f - \omega_p)}, \tag{A15}
$$

applied on the resonator at frequency $\omega_p = 2\tilde{\omega}_c$.

APPENDIX B: MASTER EQUATION

The influence of photon decay and qubit relaxation on the quantum adiabatic evolution can be studied by the master equation approach. By including photon-decay and qubit-relaxation terms, we can write the master equation [72]

$$
\begin{aligned}
\frac{d\rho_s}{dt} &= -i[H, \rho_s] + \kappa \mathcal{L}[a] + \gamma_{ge}\mathcal{L}[|g\rangle_q\langle e|] \\
&\quad + \gamma_{ef}\mathcal{L}[|e\rangle_q\langle f|] + \gamma_{gf}\mathcal{L}[|g\rangle_q\langle f|].
\end{aligned}
\tag{B1}
$$

Above, ρ_s is the density matrix of the entire system, H is the Hamiltonian of the full system given in Eq. (A9), and $\mathcal{L}[O] = O\rho O^\dagger - O^\dagger O\rho/2 - \rho O^\dagger O/2$ is the Lindbladian of the operator O. κ and γ_{jk} denote the photon decay rate of the resonator and the relaxation rate of the $(|j\rangle, |k\rangle)$ two-level systems, respectively.

To make a direct comparison of the evolution of the effective model describing by the Hamiltonian in Eq. (9) in the main text and that of our proposed full microwave-driven qutrit-resonator system described by the Hamiltonian in Eq. (A9), it is helpful to move to the rotating frame that corresponds to the interaction picture with respect to the renormalized frequency of the resonator, that is, the change of variables in Eq. (B1):

$$
\tilde{\rho}_s(t) = e^{i\tilde{\omega}_c t} \rho_s e^{-i\tilde{\omega}_c t}. \tag{B2}
$$

In this new frame, the master equation is given as

$$
\begin{aligned}
\frac{d\tilde{\rho}_s}{dt} &= -i[\tilde{H}, \tilde{\rho}_s] + \kappa \tilde{\mathcal{L}}[\tilde{a}] + \gamma_{ge}\tilde{\mathcal{L}}[|g\rangle\langle e|] \\
&\quad + \gamma_{ef}\tilde{\mathcal{L}}[|e\rangle\langle f|] + \gamma_{gf}\tilde{\mathcal{L}}[|g\rangle\langle f|],
\end{aligned}
\tag{B3}
$$

where $\tilde{\mathcal{L}}[O] = O\tilde{\rho}_s O^\dagger - O^\dagger O\tilde{\rho}_s/2 - \tilde{\rho}_s O^\dagger O/2$ and $\tilde{H} = \tilde{H}_{qr} + H_d$ with

$$\tilde{H}_{qr} = (\omega_c - \tilde{\omega}_c)a^\dagger a + \sum_{j=g,e,f} \epsilon_j |j\rangle\langle j| + \tilde{H}_c,$$

$$\tilde{H}_c = g_{ge}|g\rangle\langle e|\tilde{a}^\dagger + g_{ef}|e\rangle\langle f|\tilde{a}^\dagger + g_{gf}|g\rangle\langle f|\tilde{a}^\dagger + \text{H.c.}$$
(B4)

Here, $\tilde{a}^\dagger = e^{i\tilde{\omega}_c t}a^\dagger$ and $\tilde{a} = e^{-i\tilde{\omega}_c t}a$ are the creation and annihilation operators, respectively, for the resonator in the rotating frame.

APPENDIX C: THREE-BODY INTERACTION AMONG THE THREE RESONATORS

Here, we present a detailed derivation of the effective Hamiltonian Eq. (13) in the main text. In the displaced frame with respect to the unitary transformation

$$U(t) = e^{-\tilde{\xi}_p a_q^\dagger + \tilde{\xi}_p^* a_q},$$
$$\tilde{\xi}_p = \xi_p e^{-i\omega_d t}, \quad \xi_p = \frac{\varepsilon_p}{\omega_d - \omega_q},$$
(C1)

with $U(t)aU(t)^{-1} = a + \tilde{\xi}_p$, the Hamiltonian in Eq. (12) reads

$$H = \omega_q^{(0)}a_q^\dagger a_q + \sum_{j=1}^3 \omega_j^{(0)}a_j^\dagger a_j - E_J\left(\cos\varphi + \frac{1}{2}\varphi^2\right),$$

$$\varphi = \left[\phi_q(\tilde{a}_q^\dagger + \tilde{a}_q + \tilde{\xi}_p^* + \tilde{\xi}_p) + \sum_{j=1}^3 \phi_j(a_j^\dagger + a_j)\right],$$
(C2)

where $\tilde{a}_q^\dagger$ and $\tilde{a}_q$ are the creation and annihilation operators, respectively, for the qubit mode in the displaced frame. Assuming small phase fluctuations, we can expand the cosine up to fourth order and only keep the nonrotating terms, leading to the effective Hamiltonian [30]

$$H = \omega_q' a_q^\dagger a_q + \sum_{j=1}^3 \omega_j' a_j^\dagger a_j - E_J\left[\frac{1}{24}\varphi^4 + \mathcal{O}(\varphi^6)\right],$$
(C3)

$$H = \omega_q' a_q^\dagger a_q + K_q a_q^{\dagger 2}a_q^2 + \sum_{j=1}^3 K_{qj}a_q^\dagger a_q a_j^\dagger a_j$$

$$+ \sum_{j=1}^3 (\omega_j' a_j^\dagger a_j + K_j a_j^{\dagger 2}a_j^2) + \sum_{j\neq k} K_{jk}a_j^\dagger a_k^\dagger a_j a_k$$

$$+ |\xi_p|^2\left(2K_q a_q^\dagger a_q + \sum_{j=1}^3 K_{qj}a_j^\dagger a_j\right)$$

$$+ J_{123}(a_1^\dagger a_2^\dagger a_3 e^{-i\omega_d t} + a_1 a_2 a_3^\dagger e^{i\omega_d t}),$$
(C4)

where ω_m' ($m = q, 1, 2, 3$) is the frequency for the mth mode including a renormalization of the transition frequency coming from the normal ordering procedure of the fourth-order phase term. $K_q = -E_J\phi_q^4/4$ and $K_j = -E_J\phi_j^4/4$ are the coefficients of the self-Kerr nonlinearity associated with the qubit mode and the ith resonator, respectively. $K_{jk} = -E_J\phi_j^2\phi_k^2$ denotes the coefficient of the cross-Kerr nonlinearity between the jth resonator and the kth resonator, and $K_{qj} = -E_J\phi_q^2\phi_j^2$ represents the coefficient of the cross-Kerr nonlinearity between the qubit mode and the jth resonator. $J_{123} = -E_J\phi_1\phi_2\phi_3\phi_q\xi_p$ is three-resonator coupling strength. The term in the third line of Eq. (C4) corresponds to the ac Stark shift induced by the pump mode. Note that we have not neglected the terms like $a_1^\dagger a_2^\dagger a_3$ as well as we will choose $\omega_d = \omega_1 + \omega_2 - \omega_3$ so that these terms are resonant.

By assuming that the qubit-resonator system operates in a strongly dispersive regime and the pump mode is far detuned from the qubit mode, the qubit mode, which is initially in its ground state, will remain unexcited in the whole process. Therefore, to simply the above expression, we can safely eliminate the degrees of freedom of the qubit mode and rewrite the Hamiltonian as

$$H = \sum_{j=1}^3 (\omega_j a_j^\dagger a_j + K_j a_j^{\dagger 2}a_j^2) + \sum_{j\neq k} K_{jk}a_j^\dagger a_k^\dagger a_j a_k$$

$$+ J_{123}(a_1^\dagger a_2^\dagger a_3 e^{-i\omega_d t} + a_1 a_2 a_3^\dagger e^{i\omega_d t}),$$
(C5)

where $\omega_j = \omega_j' + |\xi_p|^2 K_{qj}$. For a realistic system, the coefficients K_j and K_{jk} are very small and one can omit these associated terms in the Hamiltonian; thus we can recover the Hamiltonian given in Eq. (13) of the main text. When the pump frequency matches the detuning of the three resonators, i.e., $\omega_d = \omega_1 + \omega_2 - \omega_3$, in the interaction picture, the Hamiltonian reads as

$$H_{\text{three body}} = J_{123}(a_1^\dagger a_2^\dagger a_3 + a_1 a_2 a_3^\dagger).$$
(C6)

By taking $E_J/2\pi = 21$ GHz and $(\phi_q, \phi_1, \phi_2, \phi_3, \xi_p) = (0.35, 0.03, 0.03, 0.03, 0.5)$, it is possible to obtain a three-resonator coupling strength $J_{123}/2\pi \approx -0.1$ MHz. These parameters also yield $K_j/2\pi \approx -4.25$ kHz and $K_{jk}/2\pi \approx -4.25$ HZ, which is rather small, as excepted. Moreover, in our protocol for implementing the resonator-based LHZ annealer, the qubit-induced self-Kerr nonlinearly is only a small correction to the Kerr term given in Hamiltonian Eqs. (7) and (A14), while for the cross-Kerr nonlinearly it has been demonstrated that the error caused by this

nonlinearity term is very small for larger α and can be compensated for by introducing additional detuning terms $\delta a_j^{\dagger} a_j$ for the Ising-problem Hamiltonian [22].

———————

[1] B. Wielinga and G. J. Milburn, Quantum tunneling in a Kerr medium with parametric pumping, Phys. Rev. A **48,** 2494 (1993).

[2] B. Wielinga and G. J. Milburn, Tunneling in the presence of driving in a cavity that contains a Kerr medium and is parametrically pumped, Phys. Rev. A **49,** 5042 (1994).

[3] C. C. Gerry and S. Rodrigues, Time evolution of squeezing and antibunching in an optically bistable two-photon medium, Phys. Rev. A **36,** 5444 (1987).

[4] G. Y. Kryuchkyan and K. V. Kheruntsyan, Exact quantum theory of a parametrically driven dissipative anharmonic oscillator, Opt. Commun. **127,** 230 (1996).

[5] W. Leoński, Fock states in a Kerr medium with parametric pumping, Phys. Rev. A **54,** 3369 (1996).

[6] K. V. Kheruntsyan, D. S. Krahmer, G. Yu. Kryuchkyan, and K. G. Petrossian, Wigner function for a generalized model of a parametric oscillator: Phase-space tristability, competition and nonclassical effects, Opt. Commun. **139,** 157 (1997).

[7] T. V. Gevorgyan and G. Yu. Kryuchkyan, Parametrically driven nonlinear oscillator at a few-photon level, J. Mod. Opt. **60,** 860 (2013).

[8] C. H. Meaney, H. Nha, T. Duty, and G. J. Milburn, Quantum and classical nonlinear dynamics in a microwave cavity, Eur. Phys. J. Quantum Technol. **1,** 7 (2014).

[9] G. H. Hovsepyan, A. R. Shahinyan, Lock Yue Chew, and G. Yu. Kryuchkyan, Phase locking and quantum statistics in a parametrically driven nonlinear resonator, Phys. Rev. A **93,** 043856 (2016).

[10] N. Bartolo, F. Minganti, W. Casteels, and C. Ciuti, Exact steady state of a Kerr resonator with one- and two-photon driving and dissipation: Controllable Wigner-function multimodality and dissipative phase transitions, Phys. Rev. A **94,** 033841 (2016).

[11] F. Minganti, N. Bartolo, J. Lolli, W. Casteels, and C. Ciuti, Exact results for Schrödinger cats in driven-dissipative systems and their feedback control, Sci. Rep. **6,** 26987 (2016).

[12] X. L. Zhao, Z. C. Shi, M. Qin, and X. X. Yi, Optical Schrödinger cat states in one mode and two coupled modes subject to environments, Phys. Rev. A **96,** 013824 (2017).

[13] H. Goto, Bifurcation-based adiabatic quantum computation with a nonlinear oscillator network, Sci. Rep. **6,** 21686 (2016).

[14] S. Puri, S. Boutin, and A. Blais, Engineering the quantum states of light in a Kerr-nonlinear resonator by two-photon driving, NPJ Quant. Informa. **3,** 18 (2017).

[15] N. Bartolo, F. Minganti, J. Lolli, and C. Ciuti, Homodyne versus photon-counting quantum trajectories for dissipative Kerr resonators with two-photon driving, Eur. Phys. J. Spec. Top. **226,** 2705 (2017).

[16] A. Gilchrist, K. Nemoto, W. J. Munro, T. C. Ralph, S. Glancy, S. L. Braunstein, and G. J. Milburn, Schrödinger cats and their power for quantum information processing, J. Opt. B: Quantum Semiclassical Opt. **6,** S828 (2004).

[17] M. Mirrahimi, Z. Leghtas, V. V. Albert, S. Touzard, R. J. Schoelkopf, L. Jiang, and M. H. Devoret, Dynamically protected cat-qubits: A new paradigm for universal quantum computation, New J. Phys. **16,** 045014 (2014).

[18] A. Das and B. K. Chakrabarti, Colloquium: Quantum annealing and analog quantum computation, Rev. Mod. Phys. **80,** 1061 (2008).

[19] F. Barahona, On the computational complexity of Ising spin glass models, J. Phys. A **15,** 3241 (1982).

[20] A. Lucas, Ising formulations of many NP problems, Front. Phys. **2,** 5 (2014).

[21] H. Goto, Z. R. Lin, and Y. Nakamura, arXiv:1707.00986.

[22] S. Puri, C. K. Andersen, A. L. Grimsmo, and A. Blais, Quantum annealing with all-to-all connected nonlinear oscillators, Nat. Commun. **8,** 15785 (2017).

[23] S. E. Nigg, N. Lörch, and R. P. Tiwari, Robust quantum optimizer with full connectivity, Sci. Adv. **3,** e1602273 (2017).

[24] K. M. Birnbaum, A. Boca, R. Miller, A. D. Boozer, T. E. Northup, and H. J. Kimble, Photon blockade in an optical cavity with one trapped atom, Nature **436,** 87 (2005).

[25] Y. X. Liu, A. Miranowicz, Y. B. Gao, J. Bajer, C. P. Sun, and F. Nori, Qubit-induced phonon blockade as a signature of quantum behavior in nanomechanical resonators, Phys. Rev. A **82,** 032101 (2010).

[26] N. Didier, S. Pugnetti, Y. M. Blanter, and R. Fazio, Detecting phonon blockade with photons, Phys. Rev. B **84,** 054503 (2011).

[27] W. Leoński and A. Kowalewska-Kudlaszyk, Quantum scissors: Finite-dimensional states engineering, Prog. Opt. **56,** 131 (2011).

[28] V. V. Albert and L. Jiang, Symmetries and conserved quantities in Lindblad master equations, Phys. Rev. A **89,** 022118 (2014).

[29] A. Miranowicz, J. Bajer, M. Paprzycka, Y. X. Liu, A. M. Zagoskin, and F. Nori, State-dependent photon blockade via quantum-reservoir engineering, Phys. Rev. A **90,** 033831 (2014).

[30] Z. Leghtas, S. Touzard, I. M. Pop, A. Kou, B. Vlastakis, A. Petrenko, K. M. Sliwa, A. Narla, S. Shankar, M. J. Hatridge, M. Reagor, L. Frunzio, R. J. Schoelkopf, M. Mirrahimi, and M. H. Devoret, Confining the state of light to a quantum manifold by engineered two-photon loss, Science **347,** 853 (2014).

[31] G. Kirchmair, B. Vlastakis, Z. Leghtas, S. E. Nigg, H. Paik, E. Ginossar, M. Mirrahimi, L. Frunzio, S. M. Girvin, and R. J. Schoelkopf, Observation of quantum state collapse and revival due to the single-photon Kerr effect, Nature **495,** 205 (2013).

[32] J. Bourassa, F. Beaudoin, J. M. Gambetta, and A. Blais, Josephson-junction-embedded transmission-line resonators: From Kerr medium to in-line transmon, Phys. Rev. A **86,** 013814 (2012).

[33] S. E. Nigg, H. Paik, B. Vlastakis, G. Kirchmair, S. Shankar, L. Frunzio, M. H. Devoret, R. J. Schoelkopf, and S. M. Girvin, Black-Box Superconducting Circuit Quantization, Phys. Rev. Lett. **108,** 240502 (2012).

[34] Y. Makhlin, G. Schön, and A. Shnirman, Quantum-state engineering with Josephson-junction devices, Rev. Mod. Phys. **73**, 357 (2001).

[35] T. Yamamoto, K. Inomata, M. Watanabe, K. Matsuba, T. Miyazaki, W. D. Oliver, Y. Nakamura, and J. S. Tsai, Flux-driven Josephson parametric amplifier, Appl. Phys. Lett. **93**, 042510 (2008).

[36] C. M. Wilson, T. Duty, M. Sandberg, F. Persson, V. Shumeiko, and P. Delsing, Photon Generation in an Electromagnetic Cavity with a Time-Dependent Boundary, Phys. Rev. Lett. **105**, 233907 (2010).

[37] W. Wustmann and V. Shumeiko, Parametric resonance in tunable superconducting cavities, Phys. Rev. B **87**, 184501 (2013).

[38] M. Reagor, H. Paik, G. Catelani, L. Sun, C. Axline, E. Holland, I. M. Pop, N. A. Masluk, T. Brecht, L. Frunzio, M. H. Devoret, L. Glazman, and R. J. Schoelkopf, Reaching 10 ms single photon lifetimes for superconducting aluminum cavities, Appl. Phys. Lett. **102**, 192604 (2013).

[39] M. Reagor, W. Pfaff, C. Axline, R. W. Heeres, N. Ofek, K. Sliwa, E. Holland, C. Wang, J. Blumoff, K. Chou, M. J. Hatridge, L. Frunzio, M. H. Devoret, L. Jiang, and R. J. Schoelkopf, Quantum memory with millisecond coherence in circuit QED, Phys. Rev. B **94**, 014506 (2016).

[40] M. Mirrahimi, Cat-qubits for quantum computation, C. R. Phys. **17**, 778 (2016).

[41] T. Orlando, J. Mooij, L. Tian, C. van der Wal, L. Levitov, S. Lloyd, and J. Mazo, Superconducting persistent-current qubit, Phys. Rev. B **60**, 15398 (1999).

[42] Y.-X. Liu, J. Q. You, L. F. Wei, C. P. Sun, and F. Nori, Optical Selection Rules and Phase-Dependent Adiabatic State Control in a Superconducting Quantum Circuit, Phys. Rev. Lett. **95**, 087001 (2005).

[43] V. E. Manucharyan, J. Koch, L. I. Glazman, and M. H. Devoret, Fluxonium: Single cooper-pair circuit free of charge offsets, Science **326**, 113 (2009).

[44] G. Zhu, D. G. Ferguson, V. E. Manucharyan, and J. Koch, Circuit QED with fluxonium qubits: Theory of the dispersive regime, Phys. Rev. B **87**, 024510 (2013).

[45] Maxime Boissonneault, A. C. Doherty, F. R. Ong, P. Bertet, D. Vion, D. Esteve, and A. Blais, Back-action of a driven nonlinear resonator on a superconducting qubit, Phys. Rev. A **85**, 022305 (2012).

[46] Z. H. Wang, C. P. Sun, and Yong Li, Microwave degenerate parametric down-conversion with a single cyclic three-level system in a circuit-QED setup, Phys. Rev. A **91**, 043801 (2015).

[47] W. Pfaff, C. J. Axline, L. D. Burkhart, U. Vool, P. Reinhold, L. Frunzio, Liang Jiang, M. H. Devoret, and R. J. Schoelkopf, Controlled release of multiphoton quantum states from a microwave cavity memory, Nat. Phys. **13**, 882 (2017).

[48] S. Rosenblum, Y. Y. Gao, P. Reinhold, C. Wang, C. Axline, L. Frunzio, S. M. Girvin, L. Jiang, M. Mirrahimi, M. H. Devoret, and R. J. Schoelkopf, arXiv:1709.05425.

[49] G. E. Santoro, R. Martoňák, E. Tosatti, and R. Car, Theory of quantum annealing of an Ising spin glass, Science **295**, 2427 (2002).

[50] V. Choi, Minor-embedding in adiabatic quantum computation: I. The parameter setting problem, Quant. Inf. Proc. **7**, 193 (2008).

[51] V. Choi, Minor-embedding in adiabatic quantum computation: II. Minor-universal graph design, Quant. Inf. Proc. **10**, 343 (2011).

[52] W. Lechner, P. Hauke, and P. Zoller, A quantum annealing architecture with all-to-all connectivity from local interactions, Sci. Adv. **1**, e1500838 (2015).

[53] In the LHZ scheme, the logical coupling $\mathcal{J}_{ij}$ is encoded in the local fields applied on the physical spin and the logical local fields h_i can be treated as a logical coupling $\mathcal{J}_{i0} = h_i$, which describes the coupling strength between the ith logical spin and an ancilla fixed spin (i.e., $|\uparrow\rangle$) labeled by 0. In this work, for clarity, we use the notation adopted in Ref. [56], where σ_i^Z represents the Pauli operator for the i physical spin on the left-hand diagonal of the triangular lattice, and also denotes the Pauli operator for the i logical spin, as shown in Fig. 4.

[54] For terms in the base of the triangular lattice, i.e., three-body terms, as shown in Fig. 4(b), by introducing a fixed physical spin $|\uparrow\rangle$ it can also be realized with four-body terms.

[55] M. Leib, P. Zoller, and W. Lechner, A transmon quantum annealer: Decomposing many-body Ising constraints into pair interactions, Quantum Science and Technology **1**, 015008 (2016).

[56] A. Rocchetto, S. C. Benjamin, and Y. Li, Stabilizers as a design tool for new forms of the Lechner-Hauke-Zoller annealer, Sci. Adv. **2**, e1601246 (2016).

[57] N. Chancellor, S. Zohren, and P. A. Warburton, Circuit design for multi-body interactions in superconducting quantum annealing system with applications to a scalable architecture, NPJ Quant. Informa. **3**, 21 (2017).

[58] A. W. Glaetzle, R. M. W. van Bijnen, P. Zoller, and W. Lechner, A coherent quantum annealer with Rydberg atoms, Nat. Commun. **8**, 15813 (2017).

[59] H. Goto, Universal quantum computation with a nonlinear oscillator network, Phys. Rev. A **93**, 050301 (2016).

[60] Z. Xiang, S. Ashhab, J. Q. You, and F. Nori, Hybrid quantum circuits: Superconducting circuits interacting with other quantum systems, Rev. Mod. Phys. **85**, 623 (2013).

[61] Z. Kurucz and K. Mølmer, Multilevel Holstein-Primakoff approximation and its application to atomic spin squeezing and ensemble quantum memories, Phys. Rev. A **81**, 032314 (2010).

[62] T. Opatrný and K. Mølmer, Spin squeezing and Schrödinger-cat-state generation in atomic samples with Rydberg blockade, Phys. Rev. A **86**, 023845 (2012).

[63] T. Brecht, W. Pfaff, C. Wang, Y. Chu, L. Frunzio, M. H. Devoret, and R. J. Schoelkopf, Multilayer microwave integrated quantum circuits for scalable quantum computing, NPJ Quant. Inf. **2**, 16002 (2016).

[64] C. Axline, M. Reagor, R. Heeres, P. Reinhold, C. Wang, K. Shain, W. Pfaff, Y. Chu, L. Frunzio, and R. J. Schoelkopf, An architecture for integrating planar and 3D cQED devices, Appl. Phys. Lett. **109**, 042601 (2016).

[65] J. R. Johansson, P. D. Nation, and F. Nori, QuTiP: An open-source Python framework for the dynamics of open

quantum systems, Compu. Phys. Commun. **183,** 1760 (2012).

[66] J. R. Johansson, P. D. Nation, and F. Nori, QuTiP 2: A Python framework for the dynamics of open quantum systems, Compu. Phys. Comm. **184,** 1234 (2013).

[67] J. Q. You, X. Hu, S. Ashhab, and F. Nori, Low-decoherence flux qubit, Phys. Rev. B **75,** 140515(R) (2007).

[68] F. Yan, S. Gustavsson, A. Kamal, J. Birenbaum, A. P. Sears, D. Hover, T. J. Gudmundsen, D. Rosenberg, G. Samach, S. Weber, J. L. Yoder, T. P. Orlando, J. Clarke, A. J. Kerman, and W. D. Oliver, The flux qubit revisited to enhance coherence and reproducibility, Nat. Commun. **7,** 12964 (2016).

[69] T. Yamamoto, K. Inomata, K. Koshino, P.-M. Billangeon, Y. Nakamura, and J. S. Tsai, Superconducting flux qubit capacitively coupled to an LC resonator, New J. Phys. **16,** 015017 (2014).

[70] K. Inomata, T. Yamamoto, P.-M. Billangeon, Y. Nakamura, and J. S. Tsai, Large dispersive shift of cavity resonance induced by a superconducting flux qubit, Phys. Rev. B **86,** 140508(R) (2012).

[71] R. Krishnan and J. A. Pople, Approximate fourth-order perturbation theory of the electron correlation energy, Int. J. Quantum Chem. **14,** 91 (1978).

[72] H. J. Carmichael, *Statistical Methods in Quantum Optics 1: Master Equations and Fokker-Planck Equations* (Springer, New York, 2002), 2nd ed.